Calorimetry at a Future Linear Collider

Steven Green
of Emmanuel College

A dissertation submitted to the University of Cambridge
for the degree of Doctor of Philosophy

Abstract

This thesis describes the optimisation of the calorimeter design for collider experiments at the future Compact LInear Collider (CLIC) and the International Linear Collider (ILC). The detector design of these experiments is built around high-granularity Particle Flow Calorimetry that, in contrast to traditional calorimetry, uses the energy measurements for charged particles from the tracking detectors. This can only be realised if calorimetric energy deposits from charged particles can be separated from those of neutral particles. This is made possible with fine granularity calorimeters and sophisticated pattern recognition software, which is provided by the PandoraPFA algorithm. This thesis presents results on Particle Flow calorimetry performance for a number of detector configurations. To obtain these results a new calibration procedure was developed and applied to the detector simulation and reconstruction to ensure optimal performance was achieved for each detector configuration considered.

This thesis also describes the development of a software compensation technique that vastly improves the intrinsic energy resolution of a Particle Flow Calorimetry detector. This technique is implemented within the PandoraPFA framework and demonstrates the gains that can be made by fully exploiting the information provided by the fine granularity calorimeters envisaged at a future linear collider.

A study of the sensitivity of the CLIC experiment to anomalous gauge couplings that effect vector boson scattering processes is presented. These anomalous couplings provide insight into possible beyond standard model physics. This study, which utilises the excellent jet energy resolution from Particle Flow Calorimetry, was performed at centre-of-mass energies of 1.4 TeV and 3 TeV with integrated luminosities of 1.5ab^{-1}

and $2ab^{-1}$ respectively. The precision achievable at CLIC is shown to be approximately one to two orders of magnitude better than that currently offered by the LHC.

Finally, a study into various technology options for the CLIC vertex detector is described.

Declaration

This dissertation is the result of my own work, except where explicit reference is made to the work of others, and has not been submitted for another qualification to this or any other university. This dissertation does not exceed the word limit for the respective Degree Committee.

Steven Green

Acknowledgements

Of the many people who deserve thanks, some are particularly prominent, such as my supervisor...

Contents

"Writing in English is the most ingenious torture ever devised for sins committed in previous lives."

— James Joyce

Chapter 1

Energy Estimators

"There, sir! that is the perfection of vessels!"
— Jules Verne, 1828–1905

This chapter outlines a procedure for calibrating the Monte-Carlo (MC) response of the linear collider detector simulations with a focus on converting the detector response into accurate energy measurements, "energy estimators", for particles showering in the calorimeters. In the particle flow paradigm, all neutral particle energies are measured using the calorimeters, which makes accurate energy estimators crucial for determining detector performance. Additionally, comparisons of particle shower energy estimators and charged particle track momenta govern the event reconstruction in PandoraPFA during the reclustering stage, which further emphasises the importance of reliable energy estimators.

1.1 Motivation

The goal of a calorimeter is to measure the energy of particles that shower within it. Particle showers are a cascade of secondary particles that are produced as a high energy particle interacts with a dense material. The energy deposits produced by a showering particle in the calorimeter are known as hits. The number of hits created by a particle shower in a calorimeter depends upon the size and shape of the particle shower and the segmentation of the calorimeter. The energy of the showering particle, $E_{Cluster}$, is determined by grouping these energy deposits together into clusters and summing their

energy

$$E_{Cluster} = \sum_{ECal\ hits,\ i} E^i_{ECal} + \sum_{HCal\ hits,\ i} E^i_{HCal}\ , \tag{1.1}$$

where E^i_{ECal} is the energy of ECal hit i and E^i_{HCal} is the energy HCal hit i. In this example, the energy deposits made by the showering particle are assumed to be split across an ECal and a HCal, therefore, the sum runs over the hits in both calorimeters. This naive energy estimator will act as a starting point for the development of more sophisticated procedures aimed at improving detector performance.

Sampling calorimeters will be used at the linear collider experiments. These calorimeters are comprised of alternating layers of active and absorber materials [1]. The absorber layers initiate particle showers and propagate their growth, while the active layers produce a signal that is proportional to the energy deposited within them. The signal produced in the active layers is measured by sampling calorimeters and used to estimate the energy deposited in the absorber layers. This estimation is made by assuming the energy deposited across a calorimeter hit, that is one active and one absorber layer, is uniform. Working under this assumption, the total calorimeter hit energy is proportional to the active layer hit energy. This estimation procedure is loosely referred to as digitisation and, in this way, the cluster energy estimator introduced above can be written as

$$E_{Cluster} = \sum_{ECal\ hits,\ i} \epsilon^i_{ECal}\alpha_{ECal} + \sum_{HCal\ hits,\ i} \epsilon^i_{HCal}\alpha_{HCal}\ , \tag{1.2}$$

where α_{ECal} and α_{HCal} are digitisation constants for the ECal and HCal respectively, ϵ^i_{ECal} is the ECal active layer hit energy for hit i and ϵ^i_{HCal} is the HCal active layer hit energy for hit i. The first stage of the calibration procedure presented in this chapter covers the determination of these digitisation constants.

Once the basic energy estimator has been calibrated, it is possible to apply more advanced procedures designed to give a compensating calorimeter response [2]. A compensating calorimeter produces an identical response to a particle shower irrespective of whether the particle shower is electromagnetic or hadronic in nature. The primary cause of the difference in the response of a calorimeter to electromagnetic and hadronic showers is the undetectable energy component that is found in hadronic showers. These undetectable energy components are energy deposits produced from a showering particle that do not produce a signal in the calorimeters. Hadronic showers contain this undetectable component due to a combination of effects such as neutrons stopping within the calorimeter

and nuclear binding energy losses. Typically, this leads to calorimeters having a weaker response to hadronic showers than to electromagnetic showers.

There are two distinct routes available for achieving a compensating response from a calorimeter: The first is hardware compensation [3], whereby calorimeters are constructed using materials that yield extra energy in response to hadronic showers, and the second is software compensation [4], whereby the uncompensated calorimetric energies for hadronic showers are modified at the software level.

A novel example of hardware compensation is the ZEUS calorimeter [3]. The ZEUS calorimeter was constructed using uranium as the absorber material. In response to neutral hadrons the uranium undergoes fission producing extra energy that increases the hadronic response of the calorimeter. The amount of uranium was carefully chosen to achieve a fully compensating calorimeter response, i.e. identical calorimeter response to electromagnetic and hadronic showers. While hardware compensation is possible for the linear collider calorimeters, restrictions on calorimeter construction and the use of a large amount of radioactive material are highly undesirable.

The linear collider lends itself to software compensation as the fine segmentation of the calorimeters and precise reconstruction of individual particles makes identification of hadronic showers, and modifying their energies, feasible. A basic form of software compensation included in the linear collider reconstruction is the modification of the electromagnetic cluster energy estimator to

$$E_{EM\ Cluster} = \sum_{ECal\ hits,\ i} E^i_{ECal}\beta^{EM}_{ECal} + \sum_{HCal\ hits,\ i} E^i_{HCal}\beta^{EM}_{HCal}\ , \tag{1.3}$$

and the hadronic cluster energy to

$$E_{Had\ Cluster} = \sum_{ECal\ hits,\ i} E^i_{ECal}\beta^{Had}_{ECal} + \sum_{HCal\ hits,\ i} E^i_{HCal}\beta^{Had}_{HCal}\ , \tag{1.4}$$

where the βs are scaling factors that are applied to the energy of clusters of calorimeter hits associated with electromagnetic and hadronic clusters in the ECal and HCal. This simple scaling of energies compensates the response of the calorimeters, which leads to better detector performance. Determination of these energy scale setting constants is the second stage of the calibration procedure that is presented in this chapter.

While this scaling of energies improves detector performance, it does not account for any changes to the β scaling factors as a function of the total energy deposited. An

energy dependence in the scaling factors is expected as the mechanisms governing the propagation of hadronic showers are sensitive to the shower energy [5]. To account for this, more sophisticated software techniques have been developed that vary the calorimeter cluster energy estimator as a function of energy to achieve a compensating response across a wider range of energies. These techniques make use of the fine segmentation of the linear collider calorimeters to identify hadronic showers. These techniques also address the problem of spuriously high energy calorimeter hits, which are caused by Landau fluctuations [6]. Landau fluctuations originate from high energy knock-on electrons appearing within particle showers [7] and can lead to overestimates of the particle shower energy if they occur in the active layers of a sampling calorimeter.

1.2 Calibration in the Particle Flow Paradigm

Calibration of the linear collider detector simulation primarily related to two processors in the software framework; the digitiser, which performs the digitisation process for sampling calorimeters, and PandoraPFA. The input to the digitiser is the active layer calorimeter hit energies and the output is the combined, active and absorber layer, calorimeter hit energies. The combined hit energies are then used by PandoraPFA for event reconstruction. Calibration of the digitiser involves determining the digitisation constants, αs, and the minimum ionising particle (MIP) scale, the average energy response on a per hit level, using the active layer calorimeter hit energies. Similarly, calibration of PandoraPFA requires setting the scaling factors, β, and the MIP response using the combined calorimeter hit energies.

The α and β constants are determined by tuning the mean of reconstructed energy distributions. A number of cuts are applied when populating these reconstructed energy distributions that ensure the relevant reconstructed energy is being tuned. The application of these cuts means that linear scaling of the α and β constants does not lead to a linear shift in the mean of the reconstructed energy distributions. Therefore, when calibrating the α and β constants an iterative approach is taken; the next iteration of the calibration constant is determined by repeating the reconstruction using the current iteration of the constant and adjusting the constant based on the mean of the reconstructed energy distribution.

Determining the MIP scale is included in the calibration procedure as it is used by PandoraPFA in the identification of muons and for applying energy thresholds designed

to limit the impact of noise. This scale is also used in the digitiser for simulating electrical noise, saturation effects in scintillator readout technologies and for applying noise vetoing energy thresholds [8]. The MIP scale characterised in the digitiser and PandoraPFA by the, non-zero, peak in the distribution of the active layer and combined calorimeter hit energies for normally incident 10 GeV μ^- respectively [7]. In the linear collider detector simulation, several realistic effects are simulated by the digitiser including saturation effects, energy thresholds, timing cuts and electrical noise. Application of these effects at this point in the software chain means that the active layer hit energies are not subject to them, while the post digitisation combined calorimeter hit energies are. Consequently, the MIP scale in PandoraPFA cannot be obtained from the digitiser MIP scale, instead both have to be independently determined.

Although this overall procedure is referred to as calibration, it is actually setting the Monte-Carlo (MC) response. In a real detector, calibration would follow the setting of the MC response and would involve calibrating the real data against this clearly defined MC response.

1.2.1 Overview of the Calibration Procedure

The calibration procedure is split into four separate operations: determination of digitisation constants (αs) in the digitiser; determination of scaling factor constants (βs) in PandoraPFA; MIP scale setting in the digitiser; and MIP scale setting in PandoraPFA. Calibration of the digitiser, digitisation constants and MIP scale, uses calorimetric energy measurements prior to any reconstruction, while calibration of PandoraPFA, scale factors and MIP scale, uses fully reconstructed particle flow objects (PFOs). As reconstructed PFOs are created using calorimetric energy measurements that have been digitised, it is wise to calibrate the digitiser before PandoraPFA, therefore, the calibration procedure is applied in the following order:

1. Setting the MIP response in the digitiser.
2. Setting the digitisation constants, αs, in the digitiser.
3. Setting the MIP response in PandoraPFA.
4. Setting the scaling factors, βs, in PandoraPFA.

1.2.2 MIP Scale Determination in the Digitiser

The MIP scale in the digitiser was determined by simulating 10 GeV μ^- events and creating a distribution of active layer calorimeter hit energies for each calorimeter in the detector simulation. When populating these distribution, a direction correction factor of $\cos(\theta)$, where θ is the incident angle of the μ^- to the calorimeter hit, was applied to account for the path length of the MIP through the active medium of the calorimeter. This correction effectively makes the muons intersect the calorimeters at normal incidence. No selection cuts were applied to the sample of muon events.

The MIP scale was determined separately for the ECal, HCal barrel, HCal endcap and HCal ring as can be seen in figure 1.1. In the digitiser software only a single HCal MIP scale, taken as the HCal barrel, was required. The HCal endcap and ring MIP scales were calculated for the purposes of the HCal ring digitisation.

1.2.3 Digitisation Implementation

This section discusses how the digitisation constants, αs, are determined. The digitisation constant for a given calorimeter depends upon several factors such as the material properties of the active and absorber layers, the magnetic field strength and energy losses occurring within the gaps in the detector. Therefore, each calorimeter in the ILD detector model has a distinct constant that must be independently determined.

1.2.3.1 ECal Digitisation Implementation

The procedure for determining the digitisation constants in the ECal involves simulation of single photons at an energy $E_{MC} = 10$ GeV. Single photons at this energy are largely contained within the ECal, as shown in figure 1.2a. This makes them ideal for isolating the ECal digitisation calibration from that of the HCal digitisation calibration. Events are only used for calibrating the ECal digitisation if they are confined to the ECal. To that extent, cuts are applied ensuring that the sum of the reconstructed energy found outside the ECal is less than 1% of E_{MC} and that the $\cos(\theta) < 0.95$, where θ is the polar angle of the photon. Photons that convert are also vetoed in this event sample at MC level. The impact of these cuts on the sum of ECal hit energies for the $E_{MC} = 10$ GeV photons is shown in figure 1.2b.

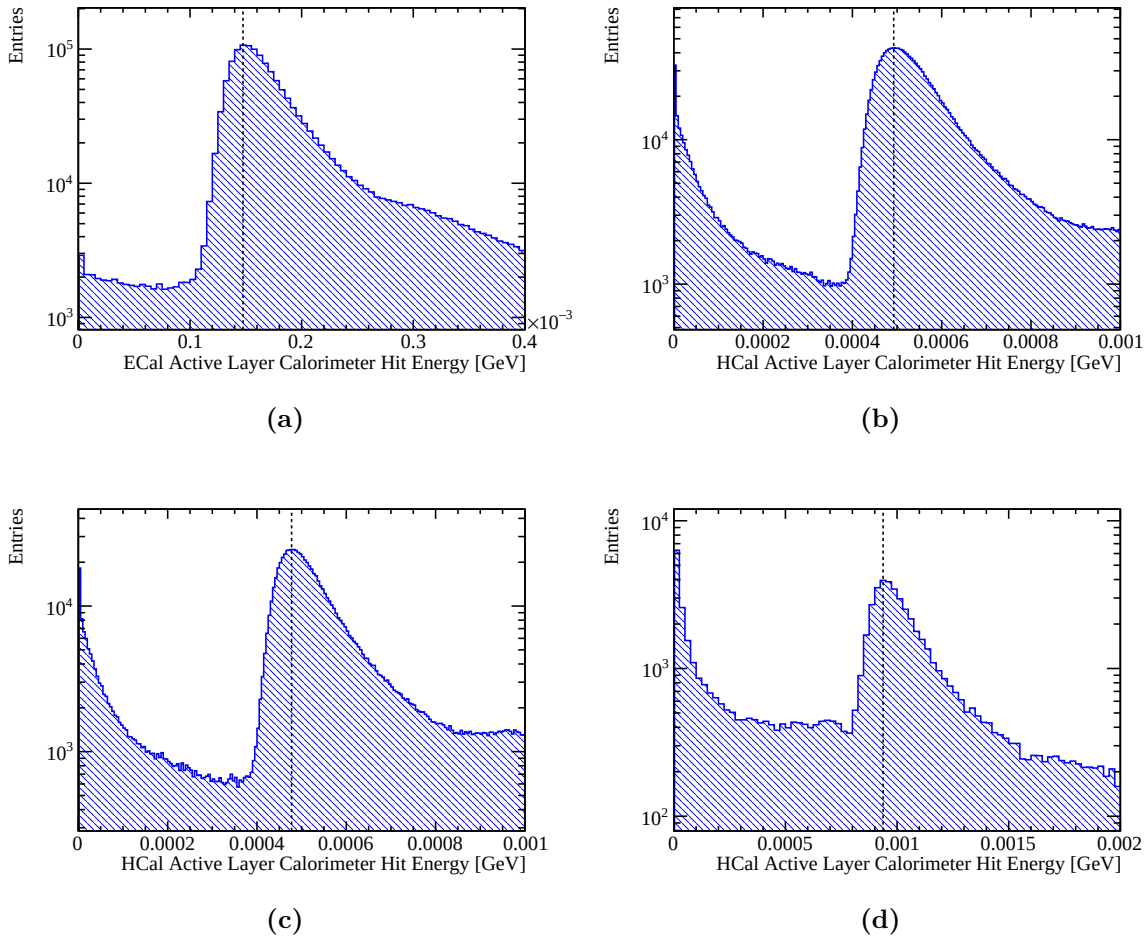

Figure 1.1: The active layer calorimeter hit energy distributions for (a) the ECal, (b) the HCal barrel, (c) the HCal endcap and (d) the HCal ring for 10 GeV μ^- events. The hit energies were corrected to account for the path length of the muons through the active medium of the calorimeter. The vertical black dotted lines indicate the position of the peak in each of these distributions that is used for defining the MIP scale in the digitisation processor.

The calibration of the digitisation in the ECal is an iterative procedure, which begins with the simulation of single photons using a trial calibration, α^0_{ECal}. Next the distribution of the sum of calorimeter hit energies within the ECal is produced for events passing the selection cuts, as shown in figure 1.2b. For an ideal calorimeter this distribution should be Gaussian, as described in chapter **??**, therefore, a Gaussian fit is applied to this distribution and the mean, E_{Fit}, extracted. To remove the effect of any outliers in this distribution, the fit is applied to the range of data with the smallest root mean square that contains at least 90 % of the data. An example of such a fit is shown in figure 1.3. In the case of ideal calibration, the mean of this fit, E_{Fit}, would be equal E_{MC}.

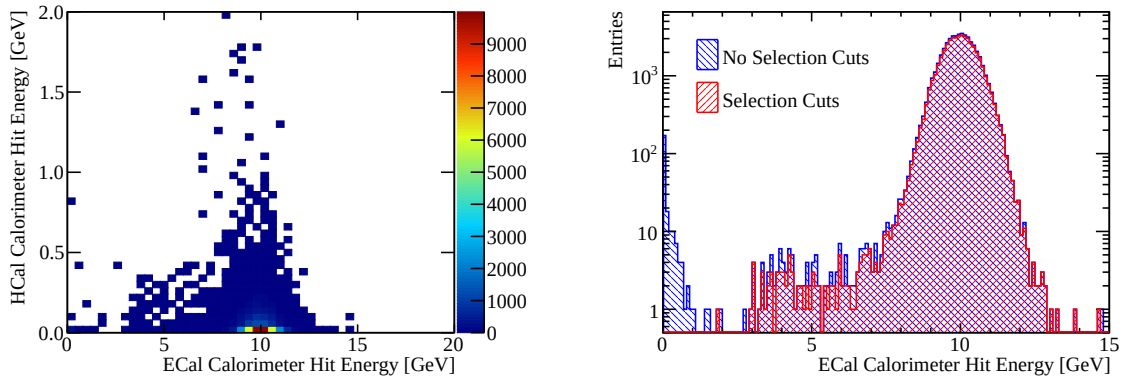

(a) **(b)**

Figure 1.2: (a) The sum of calorimeter hit energies in ECal and HCal for 10 GeV photons. (b) The sum of the ECal calorimeter hit energies for 10 GeV photons with and without the selection cuts.

It is assumed that any difference between the two is due to the calibration, therefore, to correct this the digitisation constant from the trial calibration, α^0_{ECal}, is rescaled by the ratio of the E_{MC} to E_{Fit}

$$\alpha^0_{\text{ECal}} \rightarrow \alpha_{\text{ECal}} = \alpha^0_{\text{ECal}} \times \frac{E_{MC}}{E_{Fit}} \ . \tag{1.5}$$

This procedure is then repeated until the E_{Fit} falls within a specified tolerance of E_{MC}. The tolerance applied here was $|E_{\text{Fit}} - E_{\text{MC}}| < E_{\text{MC}} \times 5\%$. The binning used for the fitted histogram is chosen such that the bin width is equal to the desired tolerance on E_{Fit} e.g. $E_{\text{MC}} \times 5\% = 0.5$ GeV. It should be emphasised that the PFO energies used for downstream analyses have the electromagnetic and hadronic energy scale corrections applied, which are calibrated to a much tighter accuracy.

1.2.3.2 HCal Digitisation Implementation

The calibration for the digitisation in the HCal proceeds in a similar manner to that described for the ECal with a few key differences. This calibration uses simulated MC long-lived neutral kaons (K^0_Ls) at $E_{MC} = 20$ GeV. The higher energy, with respect to the ECal digitisation, results in particle showers that sample deeper into the HCal. The K^0_Ls must pass through the ECal, which contains one λ_I, before arriving at the HCal. Consequently, approximately 15% of these events begin showering in the ECal, as can be

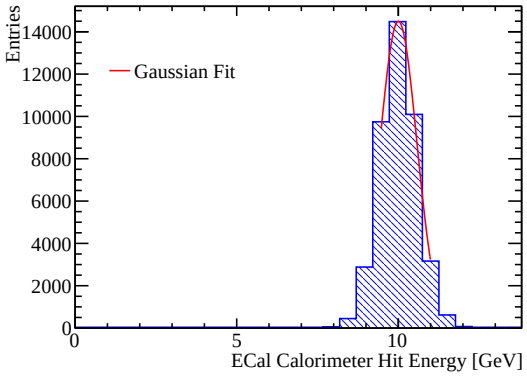

Figure 1.3: Gaussian fit to sum of the ECal calorimeter hit energies for 10 GeV photons with selection cuts. The coarse binning reflects the tolerance on the digitisation constant calibration.

seen in figure 1.4a. Only events that deposit less than 5% of their energy in the ECal are used for calibrating the HCal digitisation constants. Furthermore, events that are not contained in the HCal are removed by requiring the last layer of the HCal where energy is deposited is required to be in the innermost 90% of the HCal. The impact of these cuts on the sum of HCal calorimeter hit energies for the $E_{MC} = 20$ GeV K_L^0 events is shown in figure 1.4b.

There are two HCal digitisation constants used in the detector simulation, one applied for the barrel and another for the endcap. The use of two digitisation constants accounts for differences in hadronic shower dynamics between the two, such as differing magnetic field configurations in the barrel and endcap. Both parameters are calibrated in the same manner, but have different cuts on θ, the polar angle of the K_L^0. For the barrel region of the HCal events are selected if $0.2 < \cos(\theta) < 0.6$, while for the endcap events are selected if $0.8 < \cos(\theta) < 0.9$. These angular cuts account for the transverse profile of the hadronic showers and ensure that the showers are largely confined to the relevant sub-detector. As the majority of the neutral hadrons appearing in jets are neutrons and their accessible energy is the kinetic energy as opposed to the total energy, the target reconstructed energy for these K_L^0 samples is the kinetic energy.

After applying the above K_L^0 selection cuts, the calibration procedure for the digitisation of the HCal barrel and endcap proceeds in the same manner as was described for the ECal. An example of the Gaussian fits applied to the sum of the calorimeter hit energies in the HCal barrel and endcap are shown in figure 1.5.

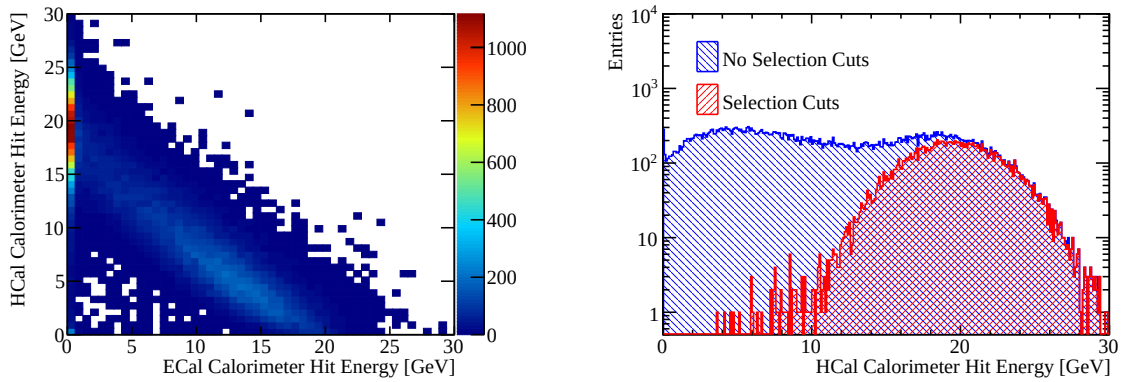

(a) **(b)**

Figure 1.4: (a) Sum of calorimeter hit energies in ECal and HCal for 20 GeV K_L^0 events. (b) Sum of the HCal calorimeter hit energies for a 20 GeV K_L^0 events with and without the selection cuts.

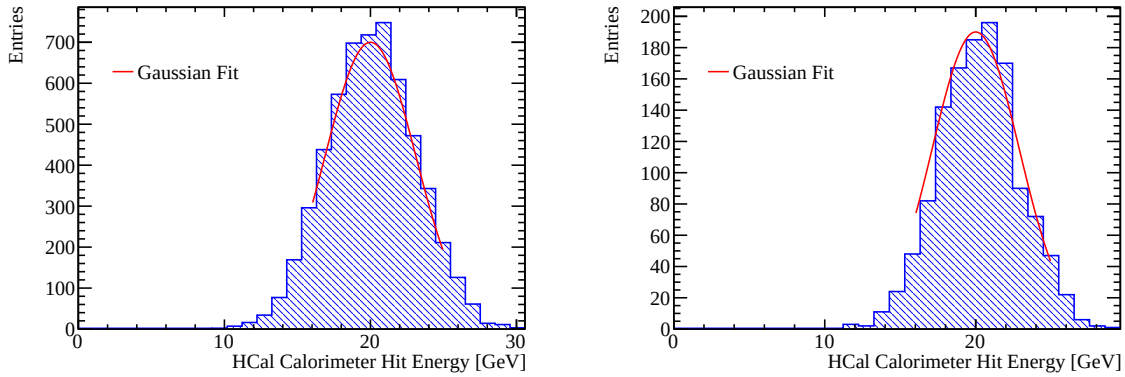

(a) HCal barrel. **(b)** HCal endcap.

Figure 1.5: Gaussian fit to sum of the HCal calorimeter hit energies for 20 GeV K_L^0 events with selection cuts.

1.2.3.3 HCal Ring Digitisation Implementation

The HCal ring, as illustrated in figure 1.6, is a hadronic calorimeter that surrounds the ECal endcap and is sandwiched between the HCal barrel and endcap. This calorimeter is required to ensure hermetic coverage of the hadronic calorimeter system across the barrel/endcap cross-over region [9].

The HCal ring has an independent digitisation constant to account for any difference in the hadronic shower development between the ring, barrel and endcap. Due to

the thickness of the HCal ring, particle showers are never fully contained in it, so a different approach to calibration is required. To ensure that the HCal ring calibration is approximately correct, $\alpha_{\text{HCal ring}}$ is assumed to equal $\alpha_{\text{HCal endcap}}$ multiplied by several factors designed to account for differences in the active layer thickness, absorber layer thickness and the MIP response between the HCal endcap and ring. In detail

$$\alpha_{\text{HCal ring}} = \alpha_{\text{HCal endcap}} \times \frac{\langle\cos(\theta_{\text{endcap}})\rangle}{\langle\cos(\theta_{\text{ring}})\rangle} \times \frac{P_{\text{endcap}}}{P_{\text{ring}}} \times \frac{L^{Absorber}_{\text{endcap}}}{L^{Absorber}_{\text{ring}}} \times \frac{L^{Active}_{\text{ring}}}{L^{Active}_{\text{endcap}}} \ , \tag{1.6}$$

where θ is the incident angle of the incoming particle to the calorimeter determined using the 20 GeV K^0_Ls, L^{Active} is the active layer thickness and $L^{Absorber}$ is the absorber layer thickness. P is the position of the MIP peak in the distribution of active layer hit energies, which has been corrected so that the MIP appears to enter the calorimeter at normal incidence, and is determined using 10 GeV μ^- events. Details on how P is determined are given in section 1.2.2.

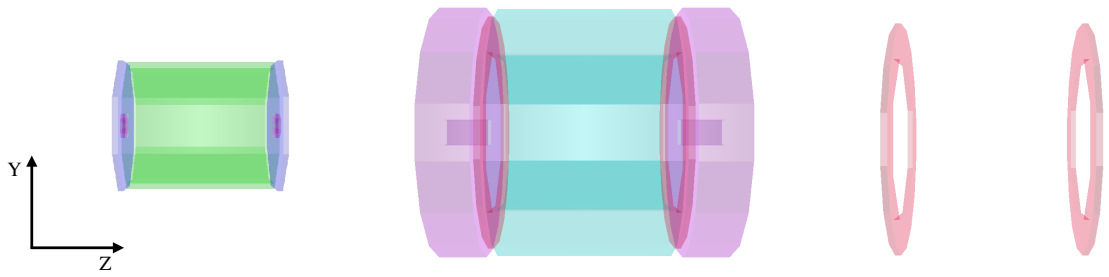

(a) **(b)** **(c)**

Figure 1.6: A PandoraPFA event display showing the nominal ILD calorimeters. (a) the ECal, (b) the full HCal and (c) the HCal ring, which covers the barrel/endcap cross-over region.

1.2.4 MIP Scale Determination in PandoraPFA

The MIP scale in PandoraPFA is set by simulating 10 GeV μ^- events and creating the distribution of combined calorimeter hit energies. The MIP scale in PandoraPFA must to be determined for the calorimeters and, in contrast to the digitiser, the muon chamber. Consequently, an additional distribution showing the calorimeter hit energy for the muon chamber must be constructed at this stage of the calibration. As was done for the digitiser, a direction correction factor was applied to the hit energies account for the

path length of the MIP through the active medium of the calorimeter and no selection cuts were applied.

Examples of the distributions used to set the MIP scale in PandoraPFA can be found in figure 1.7. Due to the energy thresholds applied in the digitiser, there are few populated low calorimeter hit energy bins in this these distributions. The double peak structure observed in the ECal calorimeter hit energy distribution is expected given the ECal absorber material thickness doubling in the back 10 layers of the ECal. The MIP peaks used for defining the MIP scale in PandoraPFA, figure 1.7, are broader than those used for determining MIP scale setting in the digitiser, 1.1, as the realistic effects applied by the digitiser are only present in the combined calorimeter hit energy distributions.

1.2.5 Electromagnetic Scale in PandoraPFA

Setting the electromagnetic scale in PandoraPFA is performed by examining the energies of fully reconstructed particles. The reconstruction was performed using the combined calorimeter hit energies that were set by the digitiser and having applied the noise vetoing MIP cuts.

The electromagnetic scale in the ECal, β_{ECal}^{EM}, is determined using simulated photons at $E_{MC} = 10$ GeV. To ensure that the events used for this part of the calibration are largely confined to the ECal, a cut requiring less than 1% of the reconstructed energy to be found outside the ECal is applied. Furthermore, only events reconstructed as a single photon are used veto conversions. The impact of the selection cuts on the electromagnetic energy measured in the ECal for 10 GeV photons is shown in figure 1.8a. The peak at zero electromagnetic energy in the ECal is due to events traveling down the beam pipe and conversions. In photon conversion events the calorimetric energy deposits made by the $e^{\pm}$ will be associated to charged particle tracks and therefore, in the particle flow paradigm, the reconstructed PFO energy will be measured using the charged particle tracks. In this case the energy measured using the calorimeters will be reported as zero, as although there are calorimetric energy deposits, they are not used when determining the PFO energies. The tail of events with low electromagnetic energy in the ECal occurs primarily due pattern recognition failures in photon conversion events. In these events a small fraction of the calorimetric energy deposits made by the $e^{\pm}$ are not associated to charged particle tracks and instead are reconstructed as separate photons with a reconstructed energy much less than E_{MC}.

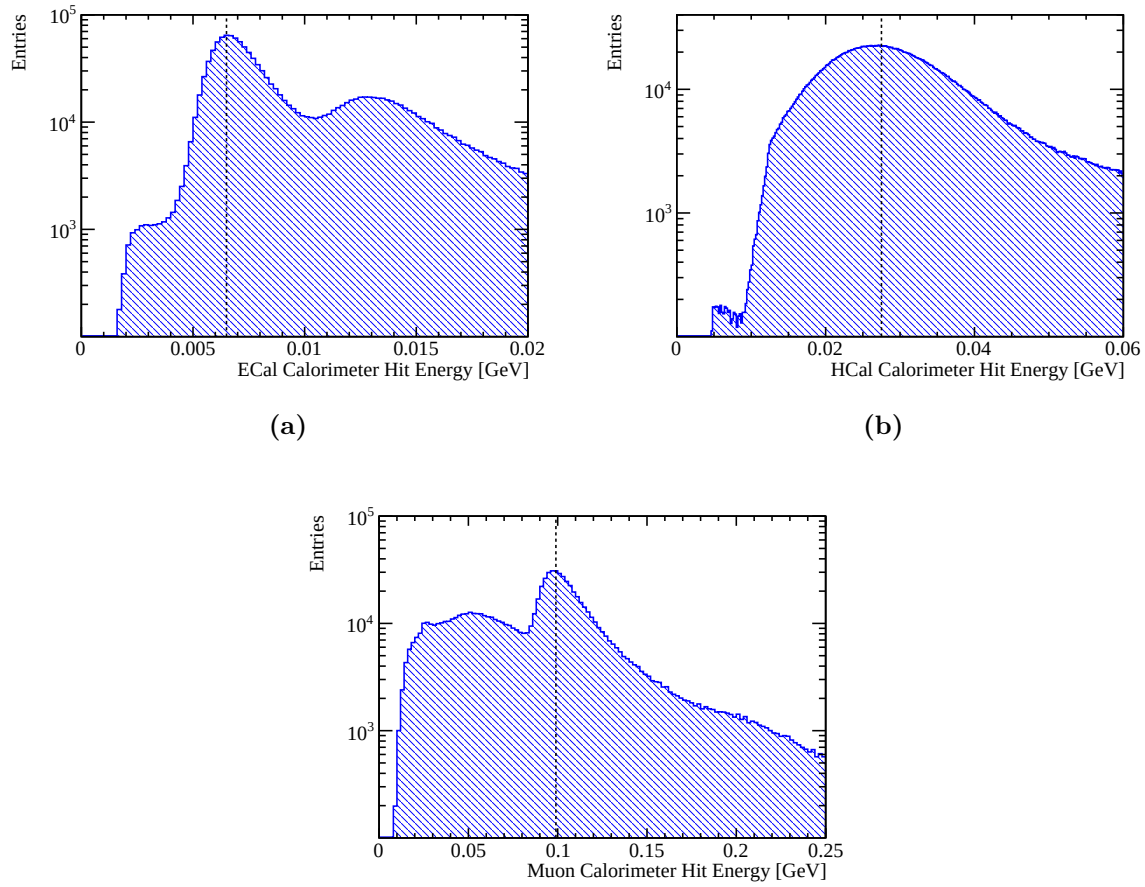

Figure 1.7: The combined calorimeter hit energy distributions for (a) the ECal, (b) the HCal and (c) the muon chamber for 10 GeV μ^- events. These hit energies were corrected to account for the path length of the muons through the active medium of the calorimeter. The vertical black dotted lines indicate the position of the peak in each of these distributions that is used for defining the MIP scale in PandoraPFA.

The fitting procedure follows that used for the ECal digitisation, described in section 1.2.3.1, whereby a trial calibration for the electromagnetic energy scale in the ECal, β_{ECal}^{EM0}, is first assumed. The initial trial calibration is approximate and will be iteratively updated until it converges to within a chosen tolerance. Using the trial calibration the photon events are reconstructed and the distribution of the electromagnetic energy in the ECal created. A Gaussian fit is then applied to this distribution in the range with the smallest root mean square containing at least 90 % of the data. The mean of the

fitted Gaussian, E_{Fit}, is then used to scale β_{ECal}^{EM0} in the following way

$$\beta_{ECal}^{EM0} \rightarrow \beta_{ECal}^{EM} = \beta_{ECal}^{EM0} \times \frac{E_{MC}}{E_{Fit}} \ . \tag{1.7}$$

An example distribution and fit used in the calibration of the nominal ILD detector model can be found in figure 1.8b. This procedure is repeated using the updated β_{ECal}^{EM} until E_{Fit} falls within a specified tolerance. The tolerance applied here was $|E_{\text{Fit}} - E_{\text{MC}}| < E_{\text{MC}} \times 0.5\%$. The binning for the fitted histogram is chosen such that the bin width is equal to the desired target tolerance on E_{Fit} e.g. $E_{\text{MC}} \times 0.5\% = 0.05$ GeV. This tolerance is tighter than was applied for the digitisation as it is these and only these energies that are used in downstream analyses.

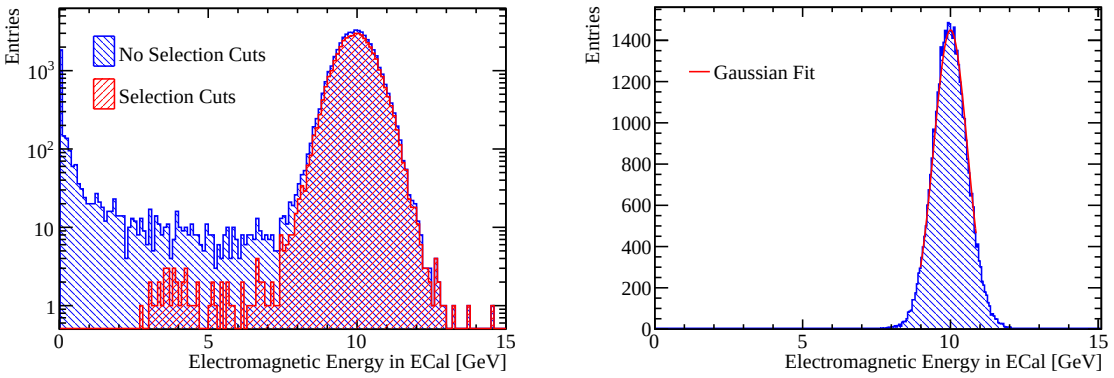

(a) **(b)**

Figure 1.8: (a) The sum of the electromagnetic energy measured in the ECal for simulated 10 GeV photons with and without the selection cuts. (b) Gaussian fit to sum of the electromagnetic energy deposited in the ECal for simulated 10 GeV photons with selection cuts.

1.2.6 Hadronic Scale in PandoraPFA

The hadronic energy scale factors for the ECal, β_{ECal}^{Had}, and HCal, β_{HCal}^{Had}, are determined using simulated K_L^0 events at $E_{MC} = 20$ GeV. As the ECal contains approximately one nuclear interaction length, a non-negligible amount of hadronic energy will be deposited in the ECal, which makes the hadronic scale in the ECal, β_{ECal}^{Had}, important for detector performance. The hadronic scale in the ECal and HCal are simultaneously set as it is unfeasible to create a large sample of 20 GeV K_L^0s that are fully contained within the ECal.

For the reasons outlined in section 1.2.3.2, the target reconstructed energy for the sample of K_L^0s used for setting the hadronic energy scale is the kinetic energy, E_K, as opposed to the total energy. To ensure the events used are not affected by leakage of energy out of the back of the HCal, a cut is applied that vetoes events where energy is deposited in the outermost 10% of the HCal. In addition, a cut requiring a single neutral hadron to be reconstructed is applied to veto events with reconstruction failures. Finally, it is required that the total hadronic energy measured within the calorimeters falls within three σ of the kinetic energy of the K_L^0, where σ is taken to be $55\% \times \sqrt{E_K}$ GeV. This definition for σ is approximately the energy resolution for neutral hadrons using the nominal ILD HCal [9]. This cut ensures that when fitting the two dimensional distribution of hadronic energy measured in the ECal and HCal, outliers do not skew the fit. The impact of these selection cuts can be seen in figure 1.9.

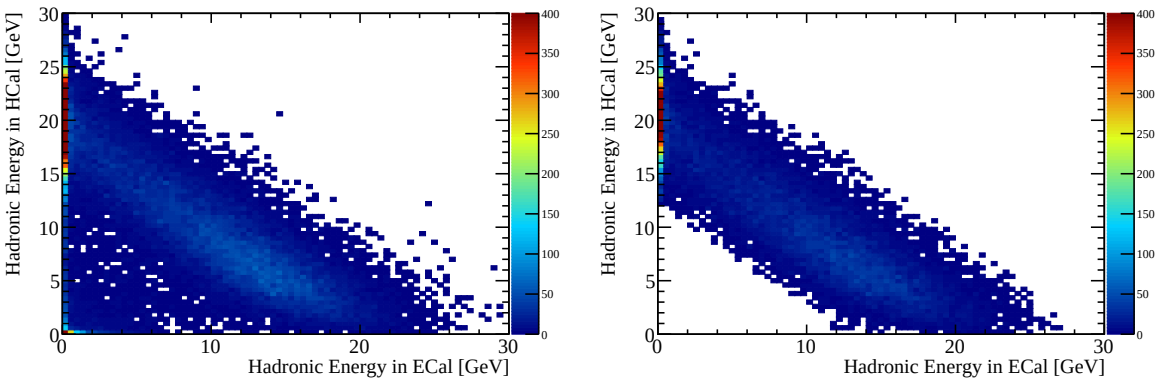

(a) **(b)**

Figure 1.9: The distribution of hadronic energy measured in the ECal and HCal for 20 GeV K_L^0 events (a) without selection cuts and (b) with selection cuts.

Determining the hadronic scale in PandoraPFA is an iterative process and begins by assuming trial values, β_{ECal}^{Had0} and β_{HCal}^{Had0}, for the hadronic scale calibration factors β_{ECal}^{Had} and β_{HCal}^{Had}. The K_L^0 events are first reconstructed using the trial scale factors. Then a linear fit is applied to the two dimensional distribution of the reconstructed hadronic energies measured in the ECal and HCal for events passing the selection cuts. The best fit is obtained by minimising χ^2 with respect to variables describing a linear fit to the distribution. In this case, χ^2 is defined as

$$\chi^2(\delta_{ECal}^{Had}, \delta_{HCal}^{Had}) = \sum_i \left(\frac{r_i}{\sigma_{r_i}} \right)^2 , \tag{1.8}$$

where r_i is the perpendicular distance in the two dimensional plane of hadronic energies measured in the ECal and HCal from the point (x_i, y_i) to a straight line passing through the points $(\delta^{Had}_{ECal}, 0)$ and $(0, \delta^{Had}_{HCal})$. In this definition, x_i and y_i are the hadronic energies measured in the ECal and HCal respectively for event i. The variables δ^{Had}_{ECal} and δ^{Had}_{HCal} describe a linear fit to the hadronic energy distribution, which are to be varied when minimising χ^2. The explicit definition of r_i is given in equation 1.9 and illustrated in figure 1.10. The uncertainty on r_i is given by σ_{r_i}, which is explicitly defined in equation 1.10. This uncertainty is calculated by propagating the uncertainties on x_i and y_i, which are assumed to be $\sigma_{x_i/y_i} = 55\% \times \sqrt{x_i/y_i}$, into the expression for r_i. The sum runs over all events, i, passing the selection cuts.

$$r_i = \frac{y_i\delta^{Had}_{ECal} + x_i\delta^{Had}_{HCal} - \delta^{Had}_{ECal}\delta^{Had}_{HCal}}{\sqrt{(\delta^{Had}_{ECal})^2 + (\delta^{Had}_{HCal})^2}} \ , \tag{1.9}$$

$$\sigma_i = \frac{(\sigma_{y_i}\delta^{Had}_{ECal})^2 + (\sigma_{x_i}\delta^{Had}_{HCal})^2}{\sqrt{(\delta^{Had}_{ECal})^2 + (\delta^{Had}_{HCal})^2}} \ . \tag{1.10}$$

The minimisation of χ^2 is done by stepping over a range of δ^{Had}_{ECal} and δ^{Had}_{HCal} centred about

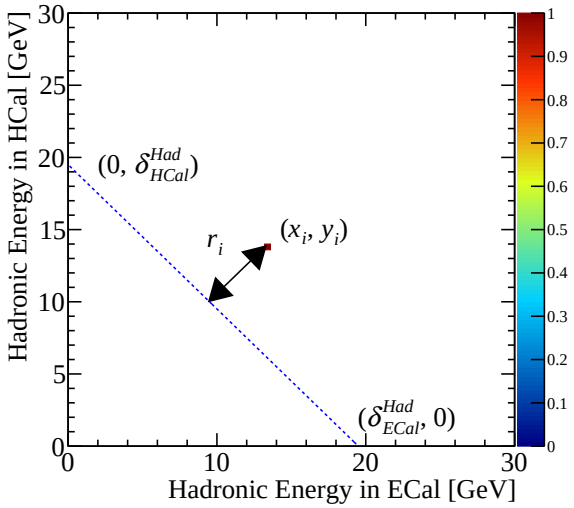

Figure 1.10: An example showing the definition of r_i. The blue dotted line corresponds to $y_i = \delta^{Had}_{HCal} - x_i\delta^{Had}_{HCal}/\delta^{Had}_{ECal}$.

the ideal value of E_K in search for the minimum χ^2. Once the minima in χ^2 is found the trial calibration factors β^{Had0}_{ECal} and β^{Had0}_{ECal} are rescaled to correct for any deviation from

the desired fit as follows

$$\beta_{ECal}^{Had0} \rightarrow \beta_{ECal}^{Had} = \beta_{ECal}^{Had0} \times \frac{E_K}{\Delta_{ECal}^{Had}} \ , \tag{1.11}$$

$$\beta_{HCal}^{Had0} \rightarrow \beta_{HCal}^{Had} = \beta_{HCal}^{Had0} \times \frac{E_K}{\Delta_{HCal}^{Had}} \ , \tag{1.12}$$

where Δ_{ECal}^{Had} and Δ_{ECal}^{Had} are the values of δ_{ECal}^{Had} and δ_{ECal}^{Had} giving the minimum χ^2. The step size used for minimising χ^2 with respect to δ_{ECal}^{Had} and δ_{ECal}^{Had} was chosen such that a single step would correspond to the final tolerance on δ^{Had}, which in this case is $\approx$ 0.1 GeV. This procedure is then repeated using the updated hadronic scaling factors until Δ_{ECal}^{Had} and Δ_{ECal}^{Had} both fall within a specified final tolerance, which in this case it taken to be $|\Delta_{E/HCal}^{Had} - E_{\mathrm{K}}| < E_{\mathrm{K}} \times 0.5\% \approx 0.1$ GeV.

The electromagnetic scale in the HCal, β_{HCal}^{EM}, is chosen to be equal to the hadronic scale in the HCal, β_{HCal}^{Had}. For the ILC and CLIC, β_{HCal}^{EM} is not a critical parameter in the reconstruction as photons are largely contained within the ECal meaning little to no electromagnetic energy is measured in the HCal.

Setting the hadronic scale in PandoraPFA ensures that the energy estimators for neutral hadrons are accurate at 20 GeV, however, this is not true for all energies. The undetectable energy component of a hadronic shower varies as a function of particle shower energy [5], which means the response of a calorimeter to neutral hadrons non-linear with the hadron energy. This is an inherent limitation of this calibration procedure that will be addressed by the development of more sophisticated energy estimators in subsequent chapters.

1.3 Conclusions

The procedure for setting the MC response in the linear collider detector simulation has been outlined. This procedure ensures that when modifying the detector simulation, the response of the detector will yield reliable energy estimators for particles showering in the calorimeter. For completion, after this calibration procedure has been applied, retraining of the likelihood data used by specific algorithms in PandoraPFA for the reconstruction of photons can be performed. The calibration procedure presented here ensures reliability when examining the performance of the linear collider detector simulation.

Chapter 2

Energy Estimators

"There, sir! that is the perfection of vessels!"
— Jules Verne, 1828–1905

2.1 Novel Energy Estimators

This section describes two novel energy estimators that are introduced with a view to improving the energy resolution for hadronic showers. Two techniques will be discussed: HCal hit energy truncation, which focuses on limiting the impact of Landau fluctuations; and software compensation, which focuses on obtaining a compensating calorimeter response. Both of these techniques are implemented by introducing weights, ω^i, to calorimetric energy deposits made by showering particles in the HCal

$$E_{Cluster} = \sum_{ECal\ hits,\ i} E^i_{ECal} + \sum_{HCal\ hits,\ i} E^i_{HCal}\omega^i(\rho^i)\ , \tag{2.1}$$

Weights are only applied to calorimeter hits in the HCal as these techniques modify the energy of hadronic showers, which are primarily contained within the HCal. The weights, ω^i, vary a function of the energy density of the calorimeter hit, $\rho^i = \frac{E^i_{HCal}}{V}$ where V is the physical volume of a calorimeter hit in the HCal, which includes the both the active and absorber layer thicknesses. While the exact weights depend on the implementation of the technique, a general feature =is that at large E^i_{HCal} the weight is less than one. This limits the impact of spuriously high energy hits caused by Landau fluctuations.

2.1.1 HCal Hit Energy Truncation

2.1.1.1 Application

The first technique to be examined is a simple truncation of the hadronic energy recorded in any given HCal hit. This improves the energy estimators for hadronic clusters by limiting the impact of Landau fluctuations. In terms of ω introduced in equation 2.1 the truncation corresponds to

$$\omega(\rho) = \begin{cases} 1 & \text{if } \rho \times V < \kappa \ , \\ \frac{\kappa}{\rho \times V} & \text{otherwise} \ , \end{cases} \tag{2.2}$$

where κ is the value of the truncation and V is the volume of a HCal hit. This weight as a function of hit energy density is shown in figure 2.1.

2.1.1.2 Results: Energy Resolution

The application of these weights leads to an improvement in the energy resolution for neutral hadrons, which can be seen in figure 2.2a. However, a great deal of care has to be given to the truncation energy so that hits from typical hadronic shower development are not truncated, while the spuriously high energy hits are. Figure 2.2a indicates that a 1 GeV truncation is sufficient for dealing with the Landau fluctuations. For hit energy truncations greater than this, the energy resolution worsens as the effect Landau fluctuations are not accounted for. For hit energy truncations below 1 GeV, the truncation is too aggressive and hits from typical hadronic shower development are truncated. For completion the γ energy resolutions as a function of HCal hit energy truncation are shown in figure 2.2b. As expected the γ energy resolution is invariant to the HCal hit energy truncation as the γs are largely contained within the ECal.

2.1.1.3 Results: Jet Energy Resolution

There is an improvement in the jet energy resolution when applying a carefully chosen HCal hit energy truncation. Figure 2.3 shows the jet energy resolution as a function of jet energy for selected values of the HCal hit energy truncation. The trends in this plot are complex as the optimal cell truncation varies with the jet energy. At low energies a 0.5 GeV truncation gives the optimal performance, however, when the jet energies

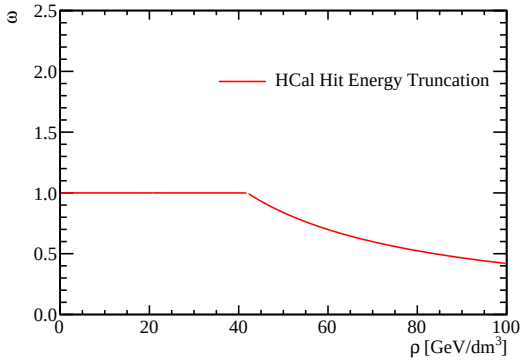

Figure 2.1: The weights, ω, used in the HCal hit energy truncation as a function of the energy density of the HCal hit, ρ. The truncation shown here corresponds to a 1 GeV truncation in the nominal ILD HCal.

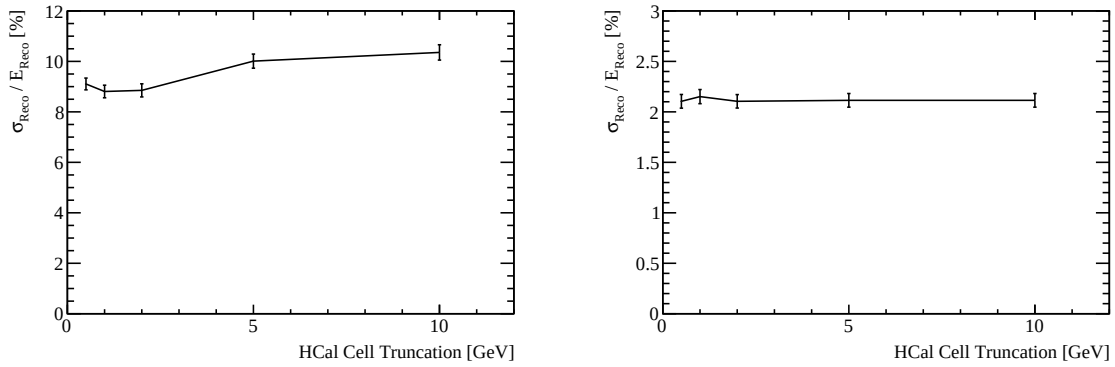

(a) **(b)**

Figure 2.2: The energy resolution as a function of HCal cell truncation for (a) 50 GeV K_L^0 events and (b) 100 GeV γ events using the nominal ILD detector model.

reach $\approx$ 180 GeV a 1 GeV truncation gives the optimal performance. This is to be expected based on the Landau fluctuations. The Landau distribution, governing the energy deposition for hadronic showers, is essentially a Gaussian with a high energy tail and as the jet energy increases, the mean of the Gaussian increases and the definition of hit energies falling in the high energy tail changes.

While it is challenging to determine the optimal truncation to use for any given detector model, it is clear that applying an appropriate truncation produces significant improvement in detector performance. Therefore, for the optimisation studies presented in chapter **??** this form of novel energy estimator is applied. The optimal truncation for each detector model considered in that study was determined by performing the

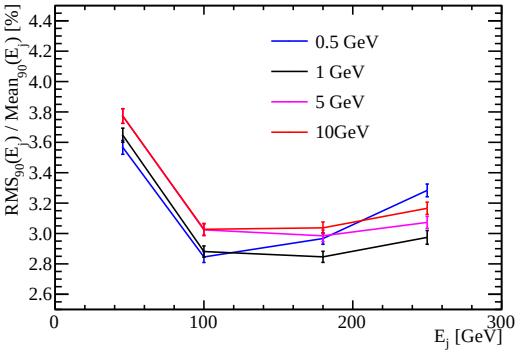

Figure 2.3: The jet energy resolution as a function of jet energy for various hadronic cell truncations. The results shown use the nominal ILD detector model.

reconstruction using range of HCal hit energy truncations and quoting the optimal performance. The HCal hit energy truncations considered in the optimisation study were 0.5, 0.75, 1, 1.5, 2, 5 and 10 GeV. For the HCal cell size study the truncation used for the 10, 20, 30, 40, 50 and 100 mm cell size detector was 0.5, 0.75, 1, 1.5, 2 and 5 GeV respectively, for the tungsten HCal options the truncation used was 5 GeV and for all other options the truncation used was 1 GeV. This optimisation has a significant impact on detector optimisation, which can be seen by comparing the jet energy resolutions obtained when using the optimised cell truncation and a fixed 1 GeV truncation, shown in figure 2.4. Without this optimisation of hit energy truncation the significance of the HCal cell size is overinflated and could lead to a misinformed detector design choice.

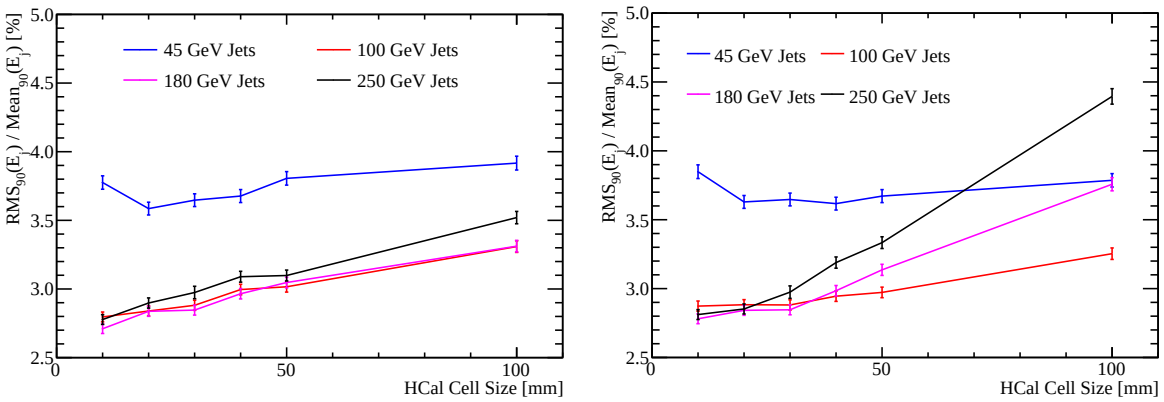

Figure 2.4: The jet energy resolution as a function of HCal cell size using a HCal hit energy truncation that is (a) optimised and (b) fixed at 1 GeV.

2.1.2 Software Compensation

2.1.2.1 Application

A particle shower produced when a hadron passing through a calorimeter has two components [5]; an electromagnetic shower core, which originates from the production and decay of π^0s and ηs, and a hadronic shower component originating from all other interacting and decaying particles in the shower. By identifying each of these components in the reconstruction, it is possible to increase the energy of the hadronic hits to give a compensating response and decrease the energy of spuriously high energy hits that come from Landau fluctuations. The challenge of applying this approach is to identify whether a hit is likely to be hadronic or electromagnetic in nature. This is done based on the energy density of a hit, with high energy densities likely to be part of the electromagnetic core and low energy densities likely to be part of satellite hadronic hits around the shower core. An event display showing the energy density of a hadronic shower, where the electromagnetic core can be clearly seen, in a 500 GeV Z→uds di-jet event can be found in figure 2.5.

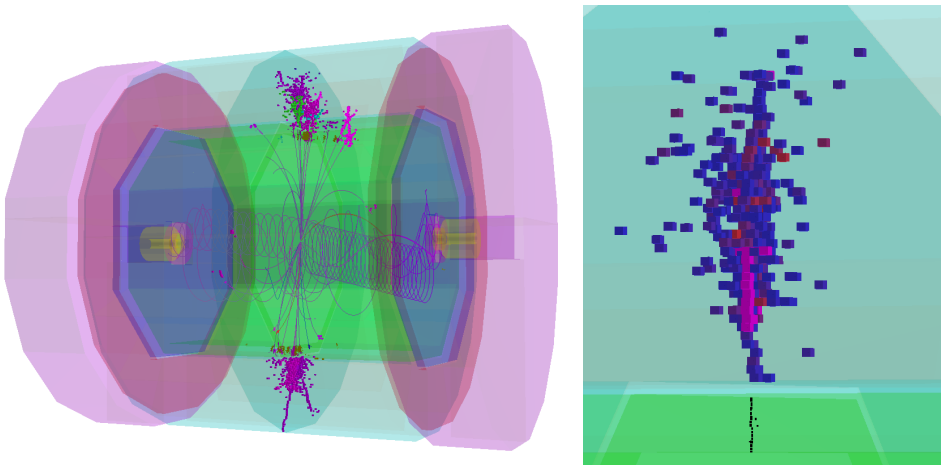

(a) **(b)**

Figure 2.5: An event display for a 500 GeV Z→uds di-jet event reconstructed using the nominal ILD detector. (a) The full event environment. (b) A single hadronic cluster from the same event where shading indicates the energy density in the HCal. High energy density cells are coloured red, while lower energy density cells are coloured blue. All ECal hits are shaded black. The high energy density electromagnetic core of the selected hadronic cluster is clearly visible.

An additional layer of sophistication in this approach is the weights that are applied vary as a function of the uncompensated cluster energy, E_{Raw}, as well as the hit energy

density, ρ^i. This is to account for any changes to the distribution of calorimeter hit energy densities as the total shower energy is varied. For example, the fraction of hits in a hadronic shower that are electromagnetic in nature increases as the total energy of the hadronic shower increases [5]. Therefore, as the total shower energy increases a smaller fraction of hits will require weights greater than one as there are less fully hadronic hits in the shower than at low energies. The highly segmented calorimeters used at the linear collider experiment will give excellent spatial resolution for individual particle showers, which enables precise mapping of the calorimeter hits to different shower components. This allows the linear collider to employ this software compensation technique with greater effectiveness than was possible for previous collider experiments.

In terms of the parameterisation introduced in equation 2.1, the weights used for this technique are [10]

$$\omega(E_{\text{Raw}}, \rho) = p_1(E_{\text{Raw}}) \times exp(p_2(E_{\text{Raw}}) \times \rho) + p_3(E_{\text{Raw}}) \tag{2.3}$$

$$p_1 = p_{11} + p_{12} \times E_{\text{Raw}} + p_{13} \times E^2_{\text{Raw}} \tag{2.4}$$

$$p_2 = p_{21} + p_{22} \times E_{\text{Raw}} + p_{23} \times E^2_{\text{Raw}} \tag{2.5}$$

$$p_3 = \frac{p_{31}}{p_{32} + exp(p_{33} \times E_{\text{Raw}})} \ , \tag{2.6}$$

where p_{ij} are trained parameters and

$$E_{Raw} = \sum_{ECal\ hits,\ i} E^i_{ECal} + \sum_{HCal\ hits,\ i} E^i_{HCal} \ . \tag{2.7}$$

The parameters p_{ij} are determined by performing a χ^2 fit of the software compensated cluster energy to the MC energy for samples of K^0_L ranging from 10 to 100 GeV in steps of 10 GeV. Using the fitted parameters obtained for the nominal ILD detector, p_1, p_2 and p_3 as a function of E_{Raw} is shown in figure 2.6 and $\omega(E_{\text{Raw}}, \rho)$ as a function of ρ for selected values of E_{Raw} is shown in figure 2.7. Figure 2.7 shows that the high energy density hits are being reduced in energy to compensate for the effects of Landau fluctuations, while the low energy density hits are being increased in weight to compensate for the invisible energy component found in hadronic showers. Furthermore, the weights vary as a function of the raw hadronic shower energy to account for the changing energy density topology of hadronic showers with increasing shower energy.

This technique is applied in the PandoraPFA framework in the form of an energy correction function, which means whenever the energy of a cluster of hits is considered by PandoraPFA the software compensated energy is used. Applying software compensation

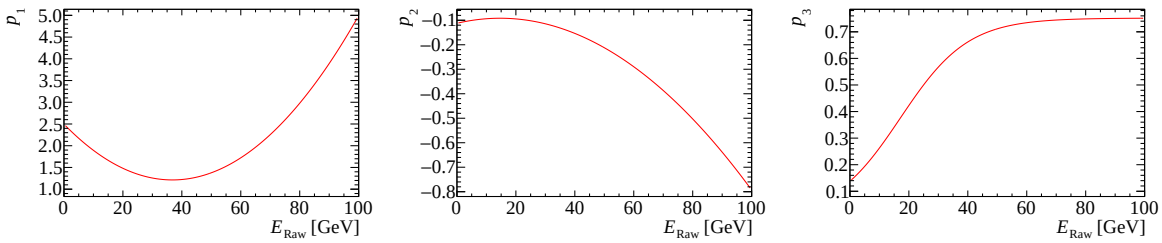

(a) **(b)** **(c)**

Figure 2.6: Parameters used in software compensation weight determination as a function of E_{Raw}.

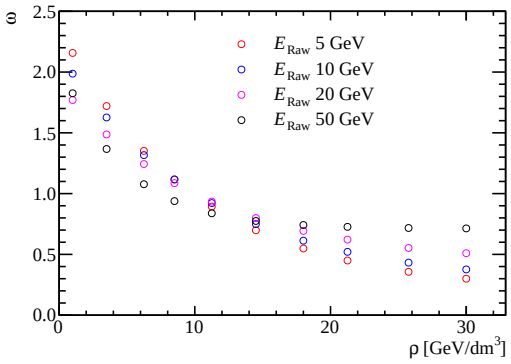

Figure 2.7: The software compensation weight applied to a calorimeter hit as a function of calorimeter hit energy density for various cluster energies.

in this way benefits the detector energy resolution in two ways; firstly, the intrinsic energy resolution of the detector improves and secondly, the confusion contribution to the energy resolution is reduced.

As software compensation only modifies the energy of HCal hits there is freedom to apply further energy corrections to the ECal hits. Applying the Clean Clusters logic, described in section 2.1.2.2, to the ECal hits alongside software compensation was found to be beneficial to the jet energy resolution. Therefore, the application of software compensation within PandoraPFA implicitly involves the application of the Clean Clusters logic to the ECal hits.

Software compensation was trained using a maximum K_L^0 energy of 100 GeV, therefore, it is only applied to clusters where $E_{\text{Raw}} < 100$ GeV as sensible behaviour outside this range cannot be ensured. While it would be possible to modify the energy range of

the training sample to go to higher energies, hadronic clusters with energy greater than 100 GeV will be rare at the ILC like energies considered here.

2.1.2.2 Context: Legacy Energy Corrections

Before examining the impact of software compensation on detector performance is it necessary to address the 'legacy' energy corrections that are used by default in PandoraPFA. The three energy correction that were in use prior to the development of software compensation are:

- **HCal hit energy truncation**, the details of which can be found in section 2.1.1.
- **Clean Clusters**. This algorithm checks to see whether the energy measured within a calorimeter hit is anomalously high. Anomalously high energy hits are defined as hits where the energy contained within the hit is greater than 10% of the energy of the cluster that the hit has been associated to. If a hit is deemed to have an anomalously high energy and if this energy is above a threshold (0.5 GeV) the hit energy used by PandoraPFA is modified. The updated hit energy is taken as the average hit energy in the calorimeter layers immediately before and after the layer containing the high energy hit.
- **Scale Hot Hadrons**. This algorithm calculates the average number of MIP equivalent particles passing through each calorimeter hit in a cluster. If this number is larger than a given value, default 15 MIPs per hit, the cluster energy is rescaled to give a lower average number of MIPs per hit, default is 5 MIPs per hit.

Each of these energy corrections help to deal with the effects of spuriously high energy hits the origin of which is described in section 2.1.1. However, the algorithms are simplistic and software compensation is expected to give far better results than these 'legacy' options. The optimisation studies presented in section **??** use all three of these legacy options simultaneously, which was the default behaviour for PandoraPFA when the studies were undertaken. The new default behaviour in PandoraPFA is to use software compensation.

2.1.2.3 Results: Energy Resolution

The energy resolution as a function of the MC energy for single K_L^0 events is shown in figure 2.8 using various energy correction settings. When comparing the energy resolution given by software compensation to that obtained using no energy corrections, it can be seen that software compensation offers a gain of $\approx 2\%$ in energy resolution across the energy range considered. The uniformity of this improvement is encouraging, indicating software compensation is achieving a compensating calorimeter response across this wide range of energies.

Comparing the performance of software compensation to the legacy corrections it can be seen that software compensation gives a better energy resolution across almost the entire range of energies considered. The only exception to this is around $E_{K_L^0} \approx$ 50 GeV where the performance of software compensation and the legacy corrections are comparable. By removing the hit truncation from the legacy options it is clear that the changes in energy resolution when using the legacy options are being driven by the hit truncation. This makes the trend in energy resolution observed using the legacy corrections clear as, at low K_L^0 energies, very few hits are affected by the truncation so the performance is comparable to not using any energy corrections. At high K_L^0 energies, the truncation is too aggressive and removes energy from hits that are not spuriously high leading to a worsening energy resolution. Between these two extremes, $E_{K_L^0} \approx 50$ GeV, the truncation works ideally and the improvement in energy resolution when using the legacy corrections is the largest.

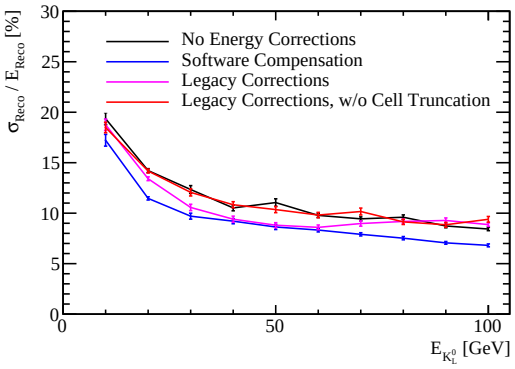

Figure 2.8: The energy resolution as a function of the MC energy for single K_L^0 events using various energy correction settings. The detector model used was the nominal ILD detector model.

2.1.2.4 Results: Jet Energy Resolution

The improvements in the intrinsic energy resolution of the detector observed when using software compensation will propagate into the reconstruction of jets. These effects are illustrated by examining the jet energy resolution as a function of jet energy, which is shown in figure 2.9. Again it is clear that software compensation is extremely beneficial to the detector performance as it gives a significant reduction in the jet energy resolution in comparison to using the legacy energy corrections.

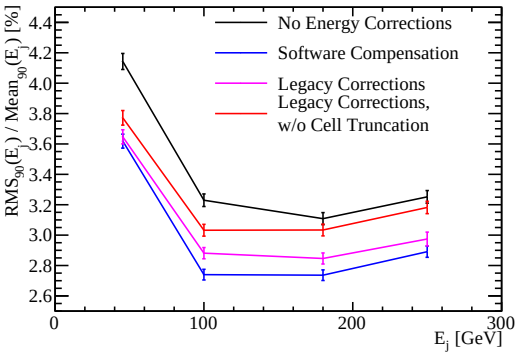

Figure 2.9: The jet energy resolution as a function of the jet energy for a variety of different energy correction options. These results were produced for the nominal ILD detector model.

Further light can be shed on these trends by examining the contributions to the jet energy resolutions from the intrinsic energy resolution and the pattern recognition confusion, which are shown in figure 2.10. The intrinsic energy resolution contribution shows that software compensation is significantly better than all other energy corrections options, which is to be expected from the energy resolution studies presented in section 2.1.2.3. Unlike the single particle study there is no jet energy for which the hit truncation matches the performance obtained using software compensation. This is due to the fact that the energy resolution when using the hit truncation is only comparable to the energy resolution using software compensation for a narrow range of hadronic cluster energies. As the jet contains a broad spectrum of hadronic cluster energies the performance obtained when using the hit truncation will always be worse than when using software compensation. When comparing the jet energy resolution for the legacy corrections is again apparent that the term driving the jet energy resolution is the hit truncation.

The confusion contributions to the jet energy resolution when using software compensation and the legacy corrections are almost identical. This indicates that the improvement

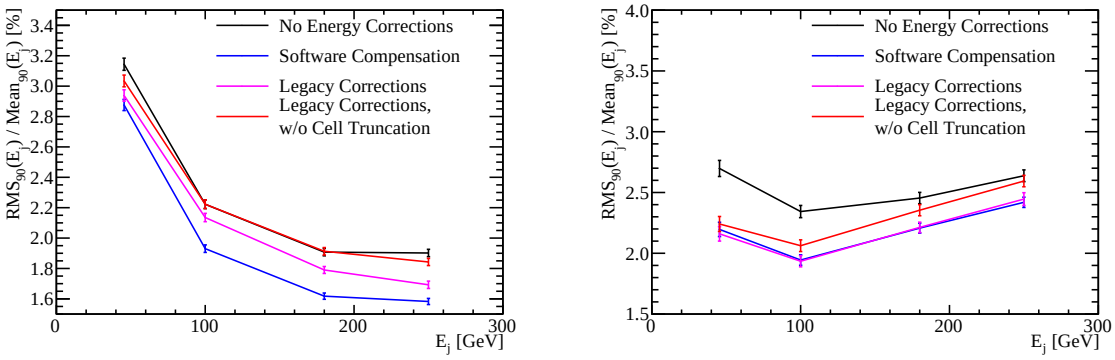

Figure 2.10: The contributions to the jet energy resolution as a function of the jet energy for a variety of different energy correction options. (a) is the intrinsic energy resolution of the detector and (b) is the total confusion term. The quadrature sum of both yields the standard reconstruction performance. These results were produced for the nominal ILD detector model.

seen in the jet energy resolution when comparing software compensation and the legacy corrections, shown in figure 2.9, is being driven by the intrinsic energy resolution. The hit truncation and software compensation techniques both improve the energy resolution of the hadronic clusters, however, software compensation is far more effective.

At low jet energies the Clean Clusters and Scale Hot Hadrons energy corrections are beneficial for reducing the confusion contribution, while the hit truncation is largely redundant. For high jet energies jets this trend is reversed. As the Clean Clusters and Scale Hot Hadrons energy corrections do not alter the intrinsic energy resolution of the detector, it is clear that they are compensating for failures in the pattern recognition, which occur primarily at low jet energies. By extracting the Clean Clusters logic, which is the driving term reducing the confusion contribution to the jet energy resolution at low jet energies, and embedding it within the software compensation energy correction, it is possible to obtain exceptional jet energy resolutions that will extend the physics reach of the linear collider detector.

2.2 Timing Cuts

The linear collider will operate using a trigger-less readout approach whereby the recorded data for each sub-detector is readout between collisions of e^+ and e^- bunches. The train

structure for ILC and CLIC, at their maximum operating energy, is shown in table 2.1. Event selection will proceed through the application of a software trigger. This involves the identification of any hard interactions, prior to full event reconstruction, and only putting data into the event reconstruction if it is measured within a chosen time window about these interactions. The recorded time of a calorimeter hit, which is cut on to make the time window for the software trigger, is corrected for straight time-of-flight to the IP. This ensures that the amount of time particle showers have to develop in the calorimeters is independent of their position in the detector. As the width of this time window changes, the amount of time particle showers have to develop changes, which will affect the performance of the detector.

	ILC 500 GeV	CLIC 3 TeV
Electrons per bunch [10^{10}]	2.0	0.37
Bunches per train	2820	312
Train repetition rate [Hz]	5	50
Bunch separation [ns]	308	0.5

Table 2.1: The train structure for 500 GeV ILC and 3 TeV CLIC [9, 11].

For all choices of time window considered in this study the calibration procedure described in section 1.2 was applied. This ensure that the mean of the reconstructed energy distributions will be invariant to changes in the calorimeter timing window as the calibration procedure compensates for any energy losses incurred by truncating the particle shower development time.

2.2.0.1 Results: Energy Resolution

The energy resolution for100 GeV γ and 50 GeV K_L^0 events as a function of the timing window applied to the calorimeter hits is shown, for the nominal ILD detector, in figure 2.11. The timing cut makes little difference to the energy resolution of the γ events, however, there is a significant decrease in the energy resolution for the neutral hadrons. This is to be expected as electromagnetic showers develop far more rapidly than their hadronic counterparts [5], which is shown in figure 2.12. Hadronic showers develop slowly as they often involve intermediate states that must decay to continue the propagation of the shower and as these states have non-zero lifetimes they slow the propagation of the shower. If a narrow calorimeter timing window is used, energy measurements from

the hadronic shower will be lost and the energy resolution will degrade, which is what is observed.

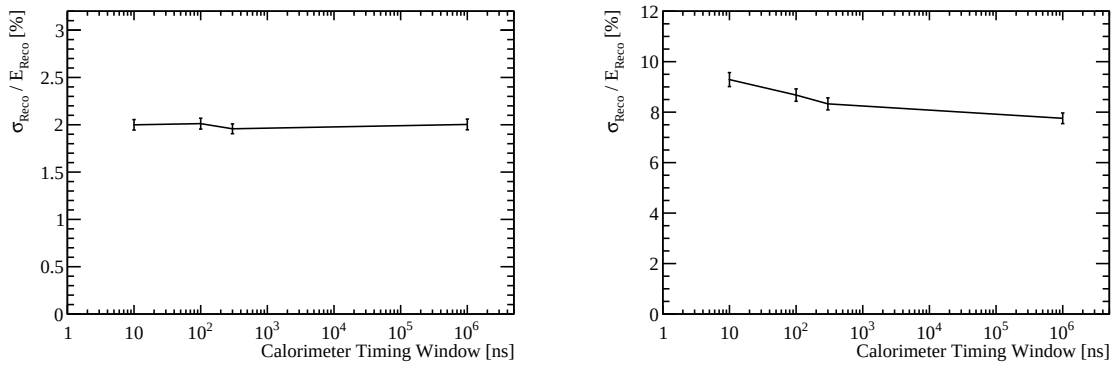

(a) **(b)**

Figure 2.11: The energy resolution as a function of calorimeter timing window for (a) 100 GeV γ events and (b) 50 GeV K_L^0 events using the nominal ILD detector model.

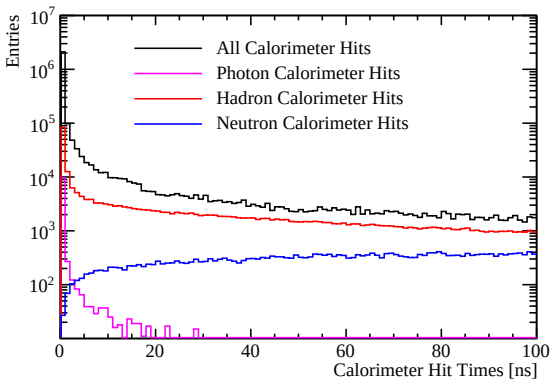

Figure 2.12: The distribution of the time of the calorimeter hits, corrected for time of flight to the impact point, for 91 GeV Z→uds di-jet events.

2.2.0.2 Results: Jet Energy Resolution

The jet energy resolution as a function of the jet energy for selected calorimeter time windows is shown in figure 2.13. As expected, the jet energy resolution will also be affected by the reduced neutral hadron energy resolution when the calorimeter timing window is reduced. The sole exception to this is the 250 GeV jets for the 100 ns time window whereby the jet energy resolution is slightly better than when using the 300 ns and semi-infinite time windows. As the magnitude of the changes to the jet energy

resolution when varying the time window size are small in comparison to the absolute resolutions, this exception will most likely be due to a fluctuation in either the event sample used or in the application of the calibration procedure.

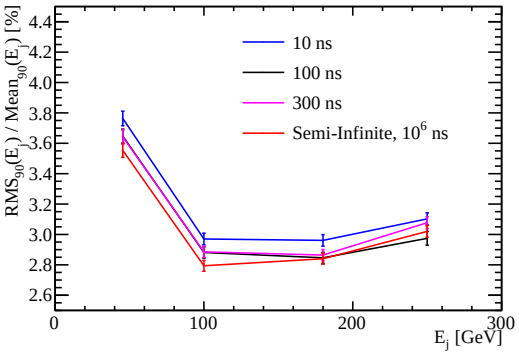

Figure 2.13: The jet energy resolution as a function of jet energy for various calorimeter timing cuts. The nominal ILD detector model was used for this study.

The time window applied to the calorimeter hits affects both the neutral hadron and jet energy resolutions with a larger timing window leading to better resolutions. It can be seen that applying an aggressive choice of time window, such as 10 ns, the jet energy resolution is degraded as many of the hadronic showers being sampled do not have time to fully develop. However, even using a 10 ns timing cut the jet energy resolutions are still sufficiently low to give excellent detector performance. Both the single particle and jet energy resolutions indicate that the majority of hadronic showers will have fully developed within 100 ns and that there are little gains to be made by extending the size of this window.

For results presented in this chapter and the optimisation studies found in chapter **??** a 100 ns timing window was applied across all models considered. As the choice of timing window has yet to be finalised for the linear collider this value was chosen as it represents something that could be achieved using the readout technology options presently available [12]. Furthermore, it adds additional realism to the detector simulation in comparison to omitting the effect of the calorimeter time window. The categorisation of changes to the detector performance when varying the calorimeter timing window presented here can be used to discern the impact of changing the timing window used for the optimisation studies at a later date if so desired.

Colophon

This thesis was made in LaTeX 2_ε using the "hepthesis" class [13].

Bibliography

[1] C. W. Fabjan and F. Gianotti. Calorimetry for particle physics. *Rev. Mod. Phys.*, 75:1243–1286, 2003.

[2] M. A. Thomson. Particle Flow Calorimetry and the PandoraPFA Algorithm. *Nucl. Instrum. Meth.*, A611:25–40, 2009.

[3] M. Derrick, D. Gacek, N. Hill, B. Musgrave, R. Noland, E. Petereit, J. Repond, R. Stanek, and K. Sugano. Design and construction of the ZEUS barrel calorimeter. *Nucl. Instrum. Meth.*, A309:77–100, 1991.

[4] Huong Lan Tran, Katja Krüger, Felix Sefkow, Steven Green, John Marshall, Mark Thomson, and Frank Simon. Software compensation in Particle Flow reconstruction. 2017.

[5] R. Wigmans. Calorimetry: Energy measurement in particle physics. *Int. Ser. Monogr. Phys.*, 107:1–726, 2000.

[6] L. Landau. On the energy loss of fast particles by ionization. *J. Phys.(USSR)*, 8:201–205, 1944.

[7] H. Bichsel, Donald E. Groom, and S. R. Klein. Passage of particles through matter. 2004.

[8] Oskar Hartbrich. AHCAL Digitisation. CALICE Spring Meeting 2015 & LCWS 2015, Tsukuba (Japan), 19 Apr 2015 - 24 Apr 2015, Apr 2015.

[9] Halina Abramowicz et al. The International Linear Collider Technical Design Report - Volume 4: Detectors. 2013.

[10] C. Adloff et al. Hadronic energy resolution of a highly granular scintillator-steel hadron calorimeter using software compensation techniques. *JINST*, 7:P09017, 2012.

[11] Lucie Linssen, Akiya Miyamoto, Marcel Stanitzki, and Harry Weerts. Physics and

Detectors at CLIC: CLIC Conceptual Design Report. 2012.

[12] C. Adloff et al. The Time Structure of Hadronic Showers in highly granular Calorimeters with Tungsten and Steel Absorbers. *JINST*, 9:P07022, 2014.

[13] Andy Buckley. The hepthesis LaTeX class.